Journal of Catalysis **201,** 13–21 (2001)
doi:10.1006/jcat.2001.3231, available online at http://www.idealibrary.com on IDEAL®

Preparation and Catalytic Properties of Single-Phase Ni–Sn Intermetallic Compound Particles by CVD of $Sn(CH_3)_4$ onto Ni/Silica

Ayumu Onda, Takayuki Komatsu,[1] and Tatsuaki Yashima

Department of Chemistry, Tokyo Institute of Technology, 2-12-1 Ookayama, Meguro-ku, Tokyo 152-8550, Japan

Received July 17, 2000; revised March 6, 2001; accepted March 22, 2001; published online May 25, 2001

The particles of each single-phase Ni–Sn intermetallic compound (IMC), Ni_3Sn, Ni_3Sn_2, and Ni_3Sn_4, have been formed on silica by chemical vapor deposition (CVD) of $Sn(CH_3)_4$ onto Ni/SiO_2. The prepared Ni–Sn IMC/SiO_2 was characterized by chemical analysis, X-ray diffraction, temperature-programmed reduction, and X-ray photoelectron spectroscopy. The results clarified that the particles on silica had the same stoichiometric Ni/Sn atomic ratio and specific bulk and surface structure as those of corresponding unsupported IMCs prepared by melting the mixture of pure Ni and Sn powder. The Ni–Sn IMC/SiO_2 was used as a catalyst for the dehydrogenation of cyclohexane. The catalytic activity of each Ni–Sn IMC/SiO_2 was much higher than that of the unsupported IMCs, whereas it was lower than that of the Ni/SiO_2 catalyst. The catalytic activities of Ni–Sn IMCs increased with the increasing Ni/Sn ratio. The selectivity of Ni_3Sn/SiO_2 and Ni_3Sn_2/SiO_2 for the formation of benzene was almost 100 C-%, even at higher conversions. The unsupported IMC catalysts also showed high selectivity to benzene, whereas Ni catalyst gave almost exclusively methane at higher conversions.

Key Words: **nickel; tin; intermetallic compound; silica; CVD; temperature-programmed reduction; cyclohexane.**

1. INTRODUCTION

Intermetallic compounds (IMCs) are compounds between two or more metal elements with simple stoichiometry. The most characteristic feature of IMCs is that their specific crystal structure is different from that of their component metals, while conventional alloys have the same crystal structure as that of either metal component. The specific crystal structure of IMCs is due to the strong interaction between their component elements. Some IMCs have unique bulk properties, such as shape memory effect, hydrogen storage ability, super conductivity, etc. In catalysis applications, many IMCs are anticipated to have unique catalytic properties because the surface atoms in IMCs should have different electronic and geometric structures from those in mono metals as well as those of bulk metals.

[1] To whom correspondence should be addressed. Fax: +81-3-5734-2758. E-mail: komatsu@chem.titech.ac.jp.

According to the reports about supported bimetallic catalysts, second elements sometimes enhance the activity, selectivity, and stability of their parent monometallic catalysts (1, 2). A typical example is Pt–Sn supported on alumina, which is known to be a good catalyst for naphtha reforming (3–5). In this catalyst system, Pt–Sn IMCs, such as $PtSn_4$, PtSn, and Pt_2Sn, have been proposed to be the active species from observation by transmission electron microscopy and energy-dispersed X-ray spectra and microbeam diffraction (6). PtSn was detected by Dautzenberg *et al*. in silica-supported Pt–Sn catalysts after H_2 reduction at 623 K for 3 h, whereas on alumina-supported ones, it was detected only after reduction at 923 K for 100 h (7). Becaud *et al*. have investigated Pt–Sn/Al_2O_3 by tin Mössbauer spectroscopy and proposed the presence of various Pt–Sn IMCs in addition to Sn^{2+} and Sn^{4+} ionic species (8). In the case of Ni–Sn/SiO_2 catalysts, the formation of various IMC phases, such as Ni_3Sn_2, Ni_3Sn_4, and NiSn, was observed by XRD (9).

Clarifying the catalytic properties of IMC would bring the possibility of providing new catalyst systems as well as information on the active species in the bimetallic catalysts. However, the catalytic properties of IMC itself have not been clarified satisfactorily. Most of the investigations on catalysis by IMC have dealt with so-called hydrogen storage alloys (10–13) because of their unique activity for hydrogen dissociation and the possibility for the stored hydrogen to participate in the reactions. On the other hand, we have already reported unique catalytic selectivities of Co–Ge (14), Pt–Ge (15), and Ni–Sn (16) IMCs, which are not hydrogen storage alloys. The IMCs containing Co or Ni show much lower activity for H_2–D_2 equilibration than pure Co or Ni but give high selectivity to ethylene in the hydrogenation of acetylene. Pt–Ge IMCs show high selectivity to butene in the hydrogenation of 1,3-butadiene. However, their catalytic activity suffers from low specific surface areas because they are prepared by melting the mixture of two component metals at higher temperatures than their melting points.

The specific adsorptive and catalytic properties were reported for the surface alloys, such as Au–Ni (17), Sn–Ni (18, 19), and Sn–Pt (20–23), with stable, designed, and

0021-9517/01 $35.00

ordered surface structure. In the case of Sn–Pt, the $p(2 \times 2)$ Pt_3Sn and $(\sqrt{3} \times \sqrt{3})R30^\circ$ Pt_2Sn surface alloys are selectively formed by the deposition of tin onto Pt(111). In the case of Sn–Ni, the $(\sqrt{3} \times \sqrt{3})R30^\circ$ Ni_2Sn surface alloy is formed on Ni(111). The catalytic properties were reported for the hydrogenation of ethylene and the dehydrogenation of cyclohexane on Sn–Pt (22) and the hydrogenolysis of *n*-butane on Sn–Pt (23).

In this study, to increase the activity of IMC catalysts, we carried out the preparation of IMC particles with high dispersion on silica. It was reported that *M*–Sn (*M* = Rh, Pt, Pd, or Ni) bimetallic catalysts were prepared by chemical vapor deposition (CVD) of an organo tin complex, such as $Sn(n\text{-}C_4H_9)_4$ and $Sn(CH_3)_4$, on M/SiO_2 (24–27). Tin species are deposited preferentially onto the particles of these noble metals during CVD because the noble metals have much higher hydrogenolysis activity than SiO_2. We applied the CVD method using $Sn(CH_3)_4$ and Ni/SiO_2 to prepare the fine particles of single-phase Ni–Sn IMC on SiO_2. The Ni–Sn system consists of three kinds of IMCs (Ni_3Sn, Ni_3Sn_2, and Ni_3Sn_4), which are Berthollide-type IMCs (28). The supported Ni–Sn IMC catalysts prepared by CVD were characterized by ICP, XRD, TPR, and XPS and used as catalysts for hydrogenation of acetylene and dehydrogenation of cyclohexane. Their catalytic activity and selectivity were compared with those of unsupported Ni–Sn IMC catalysts.

2. EXPERIMENTAL METHODS

Ni(5 wt%)/SiO_2 was first prepared by an incipient wetness method using $Ni(NO_3)_2 \cdot 6H_2O$ and silica gel (Fuji-Silysia, Caliact G6), followed by drying at 400 K for 8 h and calcination at 723 K for 4 h in air. It was then reduced with flowing H_2 (100 ml min^{-1}) at 723 K for 4 h, cooled with flowing H_2 to room temperature, and stored in air. The stored Ni/SiO_2 was again reduced in a fixed bed reactor for CVD under atmospheric pressure at 723 K with flowing H_2. CVD of $Sn(CH_3)_4$ (Soekawa Chemicals) was carried out by introducing the vapor of $Sn(CH_3)_4$ (4 kPa) onto Ni/SiO_2 at 373–523 K with H_2 as the carrier gas (30 ml min^{-1}) (29). After the CVD treatment, the temperature at the sample bed was raised to 623–1173 K in flowing H_2 (100 ml min^{-1}) and kept at the same temperature for 1 h. The sample was cooled in flowing H_2 to room temperature and stored in air.

Ni–Sn/SiO_2 with 5 wt% Ni and a Ni/Sn atomic ratio of 3 was prepared by the co-impregnation method using the aqueous solutions of $Ni(NO_3)_2 \cdot 6H_2O$ and $SnCl_2 \cdot 2H_2O$ and silica gel, followed by drying at 400 K for 8 h and calcination at 723 K for 4 h in air. The reduction of the sample was carried out with flowing H_2 (100 ml min^{-1}) at 723 K for 4 h and at 1173 K for 1 h.

Unsupported Ni–Sn IMCs, Ni_3Sn, Ni_3Sn_2, and Ni_3Sn_4 were prepared by melting the mixture of nickel (Koch Chemicals, 99.99%) and tin (Soekawa Chemicals, 99.99%) powders with an SiC electric furnace in flowing argon. The temperature was raised by 5 K min^{-1} to 1733 K to melt the mixture and kept at 1733 K for 1 h. The temperatures were lowered to 1270 K (Ni_3Sn), 1530 K (Ni_3Sn_2), and 1070 K (Ni_3Sn_4), which were lower by 50 K than the melting points of Ni_3Sn, Ni_3Sn_2, and Ni_3Sn_4, respectively, to anneal the sample at these temperatures for 8 h. The resultant ingots, cooled in flowing argon, were crushed in air and filtered into fine powder with diameters of 25–38 μm. The powder of pure nickel (Koch Chemicals, 99.99%) was also filtered, producing particles of diameters of 25–38 μm.

The above catalysts were dissolved in hydrochloric acid and the amounts of Ni and Sn in the filtered solutions were determined by ICP (Rigaku, JY38). The crystal structure was analyzed by X-ray diffraction (Rigaku, RINT2400) with an X-ray source of Cu $K\alpha$ at 40 kV and 100 mA.

XPS spectra of supported and unsupported IMCs were obtained by ESCALAB 220i (Fisons Instruments) with an X-ray source of Al $K\alpha$. The sample pressed into a pellet was put into a pretreatment chamber. Before and after the reduction treatment with flowing H_2 (101 kPa) at 873 K for 1 h, the sample was transferred into the spectrometer *in vacuo* (under 10^{-7} Pa) to measure the spectra. Binding energies were obtained using a C 1*s* peak (284.5 eV) as a standard.

The reduction behavior of the catalysts stored in air was examined by temperature-programmed reduction (TPR). Under a flowing $H_2(5\%)/N_2$ gas mixture, the temperature was raised from 300 to 873 K at a heating rate of 10 K min^{-1} and the consumption of hydrogen was continuously measured by a TCD detector. Trace amounts of oxygen and water in the H_2/N_2 gas mixture and water produced by the reduction of samples were removed by passing through the columns of OMI-1 (SPELCO) and P_2O_5 (Soekawa Chemicals), respectively.

A glass circulation system was used for the catalytic reactions. Before the catalytic reaction, IMC catalysts were reduced with H_2 (26.6 kPa) at 873 K for 0.5 h. Hydrogenation of acetylene was carried out with a mixture of C_2H_2 (2.7 kPa) and H_2 (13.3 kPa). Dehydrogenation of cyclohexane was carried out with a mixture of cyclohexane (2.7 kPa) and H_2 (16.0 kPa). The amounts of supported and unsupported catalysts were 0.050 and 0.10–0.50 g, respectively. Cyclohexane (Wako Pure Chemical Ind. 99.8%) was previously dehydrated with Molecular Sieves 5A (Wako Pure Chemical Ind.). Hydrogen was purified by passing through an Mn/SiO_2 column at room temperature and a silica gel column at 77 K. Acetylene was purified by repeating a freeze–pump–thaw cycle. The composition of gaseous hydrocarbons was monitored with an FID gas chromatograph (Shimadzu GC 8A).

3. RESULTS AND DISCUSSION

3.1. Characterization

3.1.1. Ni/Sn atomic ratio. Chemical vapor deposition (CVD) of $Sn(CH_3)_4$ onto Ni/SiO_2 was carried out to prepare the single-phase particles of Ni–Sn IMC on SiO_2. The hydrogenolysis of $Sn(CH_3)_4$ was expected to proceed selectively on metallic Ni particles because Ni usually has high activity for the hydrogenolysis reactions. Indeed, the Sn atoms were deposited on Ni particles in spite of a large surface area of uncovered SiO_2 at optimum temperature (25). The deposited Sn atoms and Ni particles are expected to form Ni–Sn IMCs with high-temperature treatment in flowing H_2 after CVD. In the case of samples with Ni/Sn atomic ratios of 3/1, 3/2, and 3/4, the bimetallic particles would be transformed into a single-phase Ni_3Sn, Ni_3Sn_2, and Ni_3Sn_4, respectively.

First, we studied the effects of CVD time, CVD temperature, and the existence of Ni particles on the amount of deposited Sn. After the reduction of Ni(5 wt%)/SiO_2 prepared by the incipient wetness method, the size of Ni particles was determined by TEM. The average diameter of Ni particles was about 9 nm, which coincided with those determined by XRD and the chemisorption of hydrogen. The Ni/Sn atomic ratios of 3/1, 3/2, and 3/4 correspond to Sn loadings of 3.2, 6.3, and 11.9 wt%, respectively. Figure 1 shows the amount of deposited Sn on Ni/SiO_2 as a function of CVD time at 423, 448, and 473 K. The amount of deposited Sn increased with an increase of CVD time at every temperature. However, the deposition rate decreased with CVD time, probably because Sn atoms gradually covered the surface of Ni. The higher the temperature, the faster the deposition rate, and the larger the amount of deposited Sn. After CVD at 423 K for 60 min or at 473 K for 10 min, the amount of deposited Sn on the catalysts was 3.2 wt%,

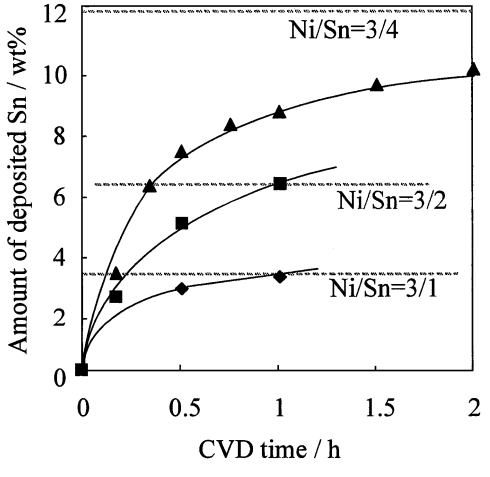

FIG. 1. Effect of CVD time on the amount of deposited Sn on Ni/SiO_2 at 423 (◆), 448 (■), and 473 K (▲). Broken lines indicate Ni/Sn atomic ratios.

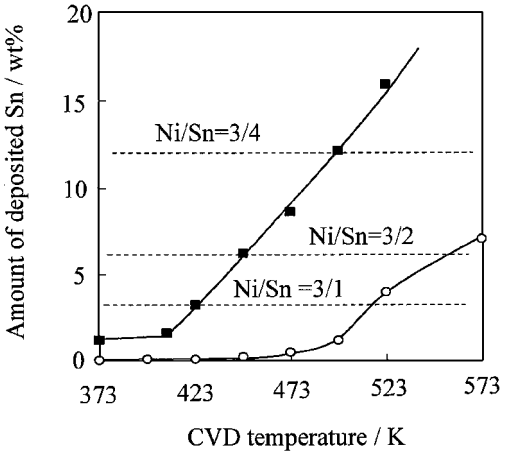

FIG. 2. Effect of CVD temperature on the amount of Sn deposited on Ni/SiO_2 (■) and SiO_2 (○) after CVD of $Sn(CH_3)_4$ for 1 h. Broken lines indicate Ni/Sn atomic ratios.

which corresponded to 3/1 of the Ni/Sn atomic ratio. If the deposited Sn atoms form monolayers only on the surface of Ni particles whose dispersion was about 10%, the amount of Sn must be below 1 wt%. However, the amount of Sn exceeded 3 wt%, even at 423 K. There could be three possible reasons for this excess deposition of Sn. The first reason is that the decomposition of $Sn(CH_3)_4$ may occur on SiO_2 as well as on Ni, even at 423 K. The second reason is that Sn atoms may be transferred from the surface of Ni particles onto SiO_2 after hydrogenolysis of $Sn(CH_3)_4$ on Ni. The third reason is that Sn atoms may enter into the bulk of Ni particles during CVD.

Figure 2 shows the amount of deposited Sn as a function of CVD temperature on Ni/SiO_2 and SiO_2, respectively. The CVD time was 1 h. The amount of deposited Sn increased with CVD temperature on both supports and was much larger on Ni/SiO_2. The amount of deposited Sn on SiO_2 was negligible below 423 K. In the case of a closed reaction system, it was reported that the dissociative adsorption of $Sn(CH_3)_4$ without H_2 on SiO_2 was observed above 473 K (30) and that no methane formation from $Sn(CH_3)_4$ and H_2 was observed on SiO_2 below 500 K (31). In our flow reaction system, the hydrogenolysis of $Sn(CH_3)_4$ proceeded preferentially on Ni particles as shown in Fig. 2. Therefore, the excess deposition of Sn atoms by CVD compared with the number of surface Ni atoms was not caused by the simultaneous deposition of Sn onto SiO_2. Figure 2 also shows that the amount of deposited Sn on Ni/SiO_2 will be continuously controlled by the CVD temperature. When CVD was carried out on Ni/SiO_2 at 423, 448, and 498 K, the Ni/Sn atomic ratio of the samples became very close to 3/1, 3/2, and 3/4, respectively.

3.1.2. Bulk structure of Ni–Sn particles. The bulk structure of samples prepared by CVD was analyzed by powder X-ray diffraction (XRD). Figure 3 shows the XRD

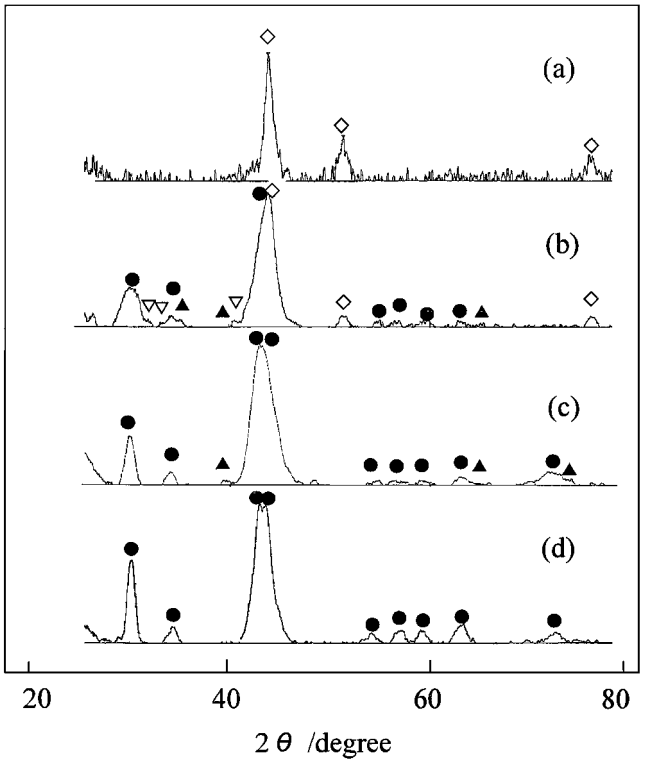

FIG. 3. XRD patterns of Ni/SiO_2 before CVD (a), and $Ni–Sn/SiO_2$ (Ni/Sn = 3/2) after CVD at 448 K (b), after subsequent hydrogen treatment at 723 K (c) and 873 K (d). ◇, Ni; ▽, β-Sn; ●, Ni_3Sn_2; ▲, Ni_3Sn_4.

patterns of parent Ni/SiO_2 (a) and $Ni–Sn/SiO_2$ (Ni/Sn = 3/2) prepared by CVD at 448 K (b) and those after the subsequent hydrogen treatment at 723 K (c) and 873 K (d). The diffraction pattern in (b) showed that the structure of Ni particles was transformed during CVD from the metallic Ni phase to a mixture of Ni_3Sn_2, Ni_3Sn_4, β-Sn, and Ni. This transformation clarified that Sn atoms entered Ni particles during CVD at 448 K, which would be the reason for the excess deposition of Sn. To obtain the single-phase Ni_3Sn_2 particles, subsequent hydrogen treatment was carried out. After hydrogen treatment at 723 K, the peaks of Ni and β-Sn disappeared but the small peaks of Ni_3Sn_4 remained in addition to the major peaks of Ni_3Sn_2. After hydrogen treatment at 873 K, the peak of Ni_3Sn_4 also disappeared and almost the same pattern was observed as that of the unsupported Ni_3Sn_2 prepared by melting the stoichiometric mixture of Ni and Sn (16). Generally, Ni_3Sn_2 is prepared above 1729 K because the melting points of Ni and Sn are 1729 and 505 K, respectively. In this study, we succeeded in the formation of single-phase Ni_3Sn_2 particles on SiO_2 by the CVD of $Sn(CH_3)_4$ and subsequent hydrogen treatment at a low temperature of 873 K, compared with the melting point of Ni, at which single-phase materials are normally produced.

Figure 4 illustrates the XRD patterns of $Ni–Sn/SiO_2$ with Ni/Sn = 3/4. The sample after CVD at 498 K (b) showed a similar pattern to that of unsupported Ni_3Sn_4, which indicates that during CVD at 498 K most of the deposited Sn entered into Ni particles to transform them into Ni_3Sn_4. The single phase Ni_3Sn_4 particles were clearly prepared by the subsequent hydrogen treatment at 723 and 873 K for 1 h (c and d). Figure 5 shows the sample with Ni/Sn=3/1. After CVD at 423 K for 1 h (b), the sample showed almost the same pattern as that of Ni/SiO_2 (a). After hydrogen treatment at 873 K (c), the Ni_3Sn phase was observed in addition to unidentified peaks. Figure 5d shows that the single-phase Ni_3Sn was formed on SiO_2 by hydrogen treatment at 1173 K for 1 h. As shown in Fig. 1, CVD at 473 K for 10 min also gave the sample with Ni/Sn = 3/1. Hydrogen treatment at 1173 K was also necessary to obtain the single-phase Ni_3Sn particles from this sample. The optimum temperature of hydrogen treatment did not depend on the CVD temperature.

It was observed that the lower the Ni/Sn ratio, the lower the temperature of hydrogen treatment necessary for the formation of single-phase Ni–Sn IMC particles: Ni_3Sn_4 (723 K), Ni_3Sn_2 (873 K), and Ni_3Sn (1173 K). The temperature of hydrogen treatment could be further lowered by using smaller parent Ni particles. The broad diffraction peaks of supported Ni–Sn IMC showed that IMC particles on SiO_2 had much smaller diameters than those of unsupported ones (16). The average particle sizes of Ni_3Sn,

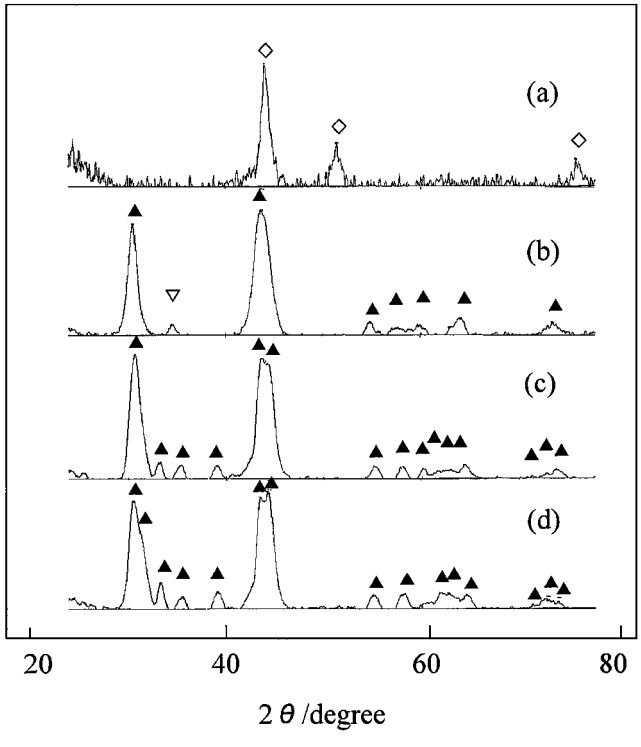

FIG. 4. XRD patterns of Ni/SiO_2 before CVD (a), and $Ni–Sn/SiO_2$ (Ni/Sn = 3/4) after CVD at 498 K (b), after subsequent hydrogen treatment at 723 K (c) and 873 K (d). ◇, Ni; ▽, β-Sn; ●, Ni_3Sn_2; ▲, Ni_3Sn_4.

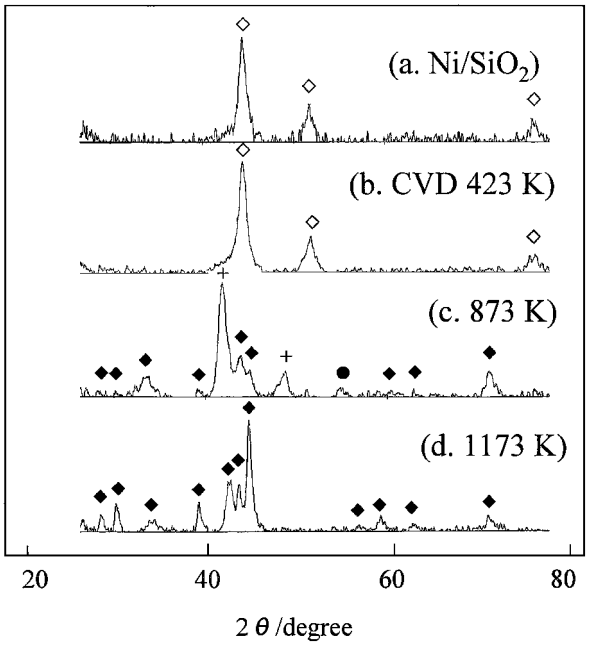

FIG. 5. XRD patterns of Ni/SiO_2 before CVD (a), and $Ni–Sn/SiO_2$ ($Ni/Sn = 3/1$) after CVD at 423 K (b), after subsequent hydrogen treatment at 873 K (c) and 1173 K (d). ◇, Ni; ◆, Ni_3Sn; ●, Ni_3Sn_2; +, unknown phase.

Ni_3Sn_2, and Ni_3Sn_4 determined by TEM were about 19, 13, and 13 nm, respectively, which coincided with those estimated by XRD. Ni_3Sn particles had the largest diameter due to hydrogen treatment of this sample being done at the highest temperature. In this study, we prepared relatively large Ni particles on SiO_2 as a starting material to obtain a clear XRD pattern. However, the use of Ni/SiO_2 with smaller Ni particles would lead to the smaller particle sizes of Ni–Sn IMC.

It is concluded that any single-phase Ni–Sn IMCs (Ni_3Sn, Ni_3Sn_2, and Ni_3Sn_4) are selectively formed on SiO_2 by the CVD of $Sn(CH_3)_4$ onto Ni/SiO_2 and subsequent hydrogen treatment at quite a lower temperature, lower than the melting point of each Ni–Sn IMC and Ni. The excess deposition of Sn compared with the surface Ni atoms is probably due in part to deposited Sn atoms entering the bulk of Ni particles during the CVD.

3.1.3. Temperature-programmed reduction (*TPR*). To clarify the reduction behavior of Ni–Sn IMC catalysts stored in air, we carried out TPR with hydrogen. As shown in Fig. 6, supported Ni (a), Ni_3Sn (b), Ni_3Sn_2 (c), and Ni_3Sn_4 (d) show their specific hydrogen consumption profiles. TPR peaks of Ni/SiO_2, Ni_3Sn/SiO_2, and Ni_3Sn_2/SiO_2 appeared at 428, 448, and 468 K, respectively. TPR profiles of unsupported catalysts are shown in Fig. 7. Peaks of Ni (a) at 428, Ni_3Sn (b) at 443 K, and Ni_3Sn_2 (c) at 468 K appeared at almost the same temperatures as those of Fig. 6a, 6b, and 6c, respectively, and would be the intrinsic peaks of Ni, Ni_3Sn, and Ni_3Sn_2 exposed in air, respectively. Therefore, Fig. 6b and 6c would indicate the formation of Ni_3Sn and Ni_3Sn_2 IMC particles, respectively. TPR of Ni_3Sn_4/SiO_2 (Fig. 6d) gave broad peaks at 523 and 653 K. These were similar to the broad peaks of unsupported Ni_3Sn_4 that appeared at 473, 573, and 623 K (Fig. 7d). Figure 6e shows the TPR of Sn/SiO_2 prepared by CVD of $Sn(CH_3)_4$ onto SiO_2 at 573 K. Sn/SiO_2 showed only sharp XRD peaks of metallic β-Sn phase. Figure 6e shows a broad peak at about 820 K. Therefore, no isolated Sn species are present on Ni_3Sn_4/SiO_2. It is clarified that the supported Ni, Ni_3Sn, Ni_3Sn_2, Ni_3Sn_4, and Sn each have an intrinsic TPR profile. The supported Ni_3Sn, Ni_3Sn_2, and Ni_3Sn_4 prepared by CVD will not include particles of pure Ni or pure Sn, and each IMC will be free from the other IMCs.

Figure 6f shows the TPR results of $Ni–Sn/SiO_2$ with $Ni/Sn = 3/1$ prepared by co-impregnation. A shoulder peak appeared at 428 K in addition to a main peak at 453 K. This shoulder would be attributed to the reduction of pure Ni particles without strong interaction with Sn. The result indicates that both particles of Ni_3Sn and Ni exist on $Ni–Sn(Ni/Sn = 3/1)/SiO_2$ prepared by co-impregnation. In this case, Sn particles, probably SnO_2, should also exist based on the stoichiometry. It is difficult to obtain the particles of single-phase Ni–Sn IMC on SiO_2 by the co-impregnation method.

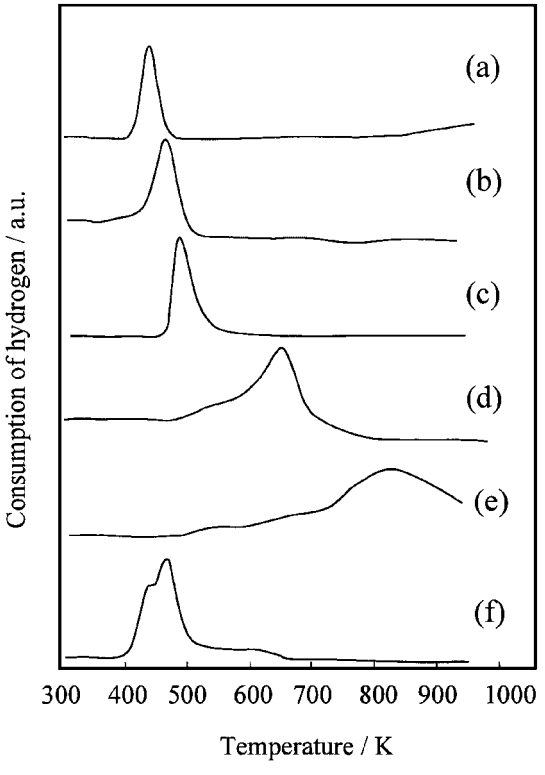

FIG. 6. TPR profiles of Ni/SiO_2 (a), $Ni–Sn$ IMC$/SiO_2$ prepared by CVD method with $Ni/Sn = 3/1$ (b), 3/2 (c), 3/4 (d), Sn/SiO_2 (e), and $Ni–Sn/SiO_2$ ($Ni/Sn = 3/1$) prepared by co-impregnation (f).

TABLE 1

X-Ray Photoelectron Spectroscopy Data

Sample	Ni $2p_{3/2}$ (eV)	Sn $3d_{5/2}$ (eV)		Ni/(Ni + Sn)/ (at.%)	Reference
	Ni^0	Sn^0	Sn^{2+}, Sn^{4+}		
Ni/SiO_2	852.8	—	—	—	This work
Ni_3Sn/SiO_2	852.7	485.0	—	56	This work
Ni_3Sn_2/SiO_2	852.5	485.3	—	48	This work
Ni_3Sn_4/SiO_2	852.4	484.3	486.7	22	This work
Sn/SiO_2	—	—	486.8	—	This work
Ni	852.8	—	—	—	(16)
Ni_3Sn	852.6	485.0	—	57	(16)
Ni_3Sn_2	852.7	485.0	—	42	(16)
Ni_3Sn_4	852.6	484.9	—	28	(16)
Sn	—	485.0	486.8	—	(32)

3.1.4. X-ray photoelectron spectroscopy (XPS). Table 1 shows XPS results for the supported Ni–Sn IMC after reduction with hydrogen at 873 K. The binding energy of Ni $2p_{3/2}$ for Ni/SiO_2 was 852.8 eV, which indicates that the Ni particle is metallic. However, the binding energy of Sn $3d_{5/2}$ for Sn/SiO_2 prepared by CVD was 486.8 eV, which indicates that the surface Sn atoms are not reduced to Sn^0 by reduction at 873 K. The binding energies of Ni and Sn for Ni_3Sn/SiO_2 and Ni_3Sn_2/SiO_2 clarified the reduction to Ni^0 and Sn^0. In the case of Ni_3Sn_4/SiO_2, some of the surface Sn atoms were not reduced to Sn^0. However, in the cases of unsupported Ni_3Sn, Ni_3Sn_2, and Ni_3Sn_4, Sn atoms were completely reduced to Sn^0 (16). Therefore, Ni_3Sn_4/SiO_2 may contain a small number of Sn atoms that do not constitute Ni_3Sn_4.

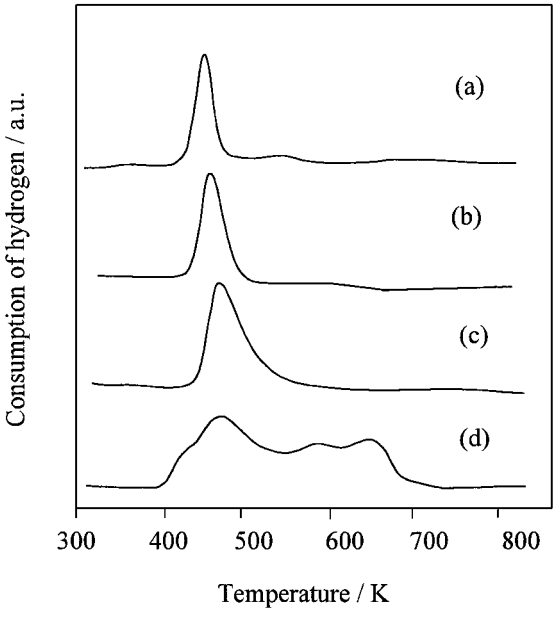

FIG. 7. TPR profiles of unsupported Ni (a), Ni_3Sn (b), Ni_3Sn_2 (c), and Ni_3Sn_4 (d).

The binding energies of Ni $2p_{3/2}$ (852.7 eV) and Sn $3d_{5/2}$ (485.0 eV) for Ni_3Sn/SiO_2 and Ni $2p_{3/2}$ (852.5 eV) and Sn $3d_{5/2}$ (485.3 eV) for Ni_3Sn_2/SiO_2 were almost the same as those for metallic Ni and Sn (32). Almost the same binding energies were reported for the unsupported Ni–Sn IMCs (16). Therefore, the electronic interaction between Ni and Sn was not obvious in the binding energies of Ni 2*p* and Sn 3*d*. However, for the unsupported Ni–Sn IMCs, we have already reported that the XPS spectra of Ni 3*d* near the Fermi level exhibit the following changes with increasing tin content; the density of states at Fermi level decreases, the shape of Ni 3*d* peak narrows, and the peak top shifts toward higher binding energy (16). The peak narrowing would be due to the localization of free electrons. The shift toward higher binding energy would be due to the filling of Ni 3*d* orbital with electrons transferred from tin. These two changes could result in the decrease in density of states at the Fermi level (16). Similar XPS spectra near the Fermi level are expected to be observed for the supported Ni–Sn IMCs.

The proportions of Ni near the surface of the supported and unsupported Ni–Sn IMCs are shown in Table 1 as Ni/(Ni + Sn) determined from the peak areas of Ni $2p_{3/2}$ and Sn $3d_{5/2}$ XPS spectra. The actual proportion may be higher than the values in Table 1 because it is difficult to integrate completely the areas of the Ni $2p_{3/2}$ peak containing many satellite peaks. The Ni/(Ni + Sn) values of Ni_3Sn/SiO_2, Ni_3Sn_2/SiO_2, and Ni_3Sn_4/SiO_2 were 56, 48, and 22 at.%, respectively, whereas those of unsupported Ni_3Sn, Ni_3Sn_2, and Ni_3Sn_4 were 57, 42, and 28 at.%, respectively. The XPS data would clarify that each Ni–Sn IMC, with the identical bulk atomic ratio, has almost the same surface composition for both the supported and unsupported Ni–Sn IMC catalysts.

3.2. Catalytic Reactions

3.2.1. Hydrogenation of acetylene. The catalytic properties of silica-supported Ni–Sn IMC prepared by the CVD method for acetylene hydrogenation were compared with those of unsupported IMC, supported Ni–Sn prepared by co-impregnation, and pure Ni. We have already reported that the unsupported Ni–Sn IMC catalysts catalyze the partial hydrogenation of acetylene into ethylene because of their extremely low activity for ethylene hydrogenation (16). In contrast, over the Ni catalyst, ethylene hydrogenation proceeds faster than acetylene hydrogenation (16, 33).

Selectivity to ethylene is summarized in Table 2. Ethylene selectivity is expressed by the molar ratio of ethylene/(ethylene + ethane) obtained at the reaction time when acetylene was completely converted. The reaction temperature was different for each catalyst because of the large difference in catalytic activity. Over unsupported Ni, ethylene selectivity was 65%, whereas over both the unsupported Ni_3Sn and Ni_3Sn_2, the selectivity was about 100%.

TABLE 2

Selectivity of Various Catalysts in Acetylene Hydrogenation

Catalysts	Ethylene[a] selectivity (%)	Reaction temperature (K)
Unsupported Ni	65	398
Ni/SiO_2	50	343
Unsupported Ni_3Sn	100	523
Ni_3Sn/SiO_2[b]	96	448
Ni_3Sn/SiO_2[b]	88	398
$Ni–Sn(Ni/Sn = 3)/SiO_2$[c]	65	398
Unsupported Ni_3Sn_2	100	523
Ni_3Sn_2/SiO_2[b]	98	448

[a] Ethylene/(ethylene + ethane) molar ratio obtained when acetylene was converted completely.
[b] Prepared by CVD method.
[c] Prepared by co-impregnation.

In the case of the supported catalysts, Ni_3Sn/SiO_2 showed high ethylene selectivity, 96% at 448 K and 88% at 398 K, and Ni_3Sn_2/SiO_2 also showed high selectivity, 98%. In contrast, over supported Ni–Sn (Ni/Sn = 3) prepared by co-impregnation, ethylene selectivity was quite similar to Ni, indicating the presence of Ni particles as was suggested by TPR. The reaction temperature in Table 2 shows that these supported catalysts have much higher activity than the unsupported ones. In the case of Ni_3Sn_4, unsupported Ni_3Sn_4 did not show any activity at 523 K for 2 h (16) and Ni_3Sn_4/SiO_2 exhibited very low acetylene hydrogenation activity at 473 K. For the supported catalysts, the order of the activity for acetylene hydrogenation was as follows:

$$Ni/SiO_2 > Ni_3Sn/SiO_2 > Ni_3Sn_2/SiO_2 > Ni_3Sn_4/SiO_2.$$

This order is the same as that of unsupported catalysts (16). The activity was reduced by increasing the proportion of tin in the IMC.

3.2.2. Dehydrogenation of cyclohexane. We carried out the reaction of cyclohexane in the presence of hydrogen over pure Ni and Ni–Sn IMCs. When the cyclohexane was introduced without hydrogen, methane was mainly formed over Ni catalysts. The formation of methane stoichiometrically means that coke was formed on the Ni catalysts. Actually, the Ni catalysts rapidly lost their catalytic activity for the reaction of cyclohexane without hydrogen. Therefore, hydrogen was mixed in the reactant with the initial hydrogen to cyclohexane molar ratio of 6. Figure 8 shows the results of unsupported Ni and unsupported Ni_3Sn catalysts at 823 K. The catalytic activity of Ni_3Sn was lower than that of Ni. Benzene was formed as an initial product over Ni. However, benzene was further converted into methane through hydrogenolysis, resulting in almost 100 C-% selectivity to methane at higher conversions. In contrast, Ni_3Sn converted cyclohexane into benzene but exhibited very low hydrogenolysis activity into methane, even at higher conversions. High selectivity to benzene is revealed to be characteristic of catalysis with Ni_3Sn. This catalytic property could be explained by the assumption that the surface of Ni_3Sn does not contain any Ni ensembles that have multifold coordination sites. Both the unsupported Ni_3Sn_2 and Ni_3Sn_4 showed quite low activity.

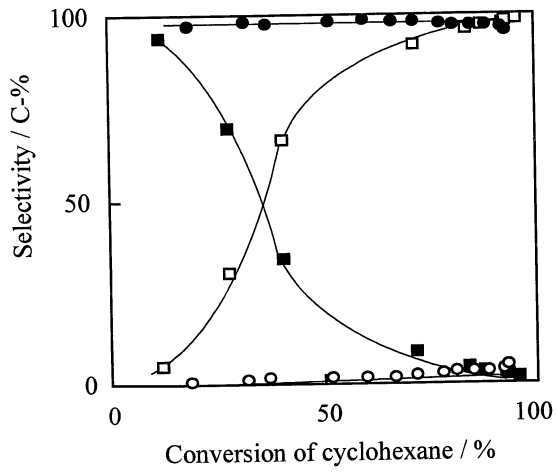

FIG. 8. Selectivity in the reaction of cyclohexane on unsupported Ni (■, C_6H_6; □, CH_4) and Ni_3Sn (●, C_6H_6; ○, CH_4) powder catalysts at 823 K. $P(H_2) = 16.0$ kPa; P(cyclohexane) = 2.7 kPa.

As clearly shown in Fig. 9, Ni_3Sn/SiO_2 showed almost the same selectivity as the unsupported Ni_3Sn catalyst and totally different selectivity from that over Ni catalysts. This result suggests that Ni particles, even if they are too small to be detected by XRD, do not exist in any applicable amount on the Ni_3Sn/SiO_2 catalyst. Ni_3Sn_2/SiO_2 showed almost the same selectivity to benzene as Ni_3Sn/SiO_2. Ni_3Sn_4/SiO_2

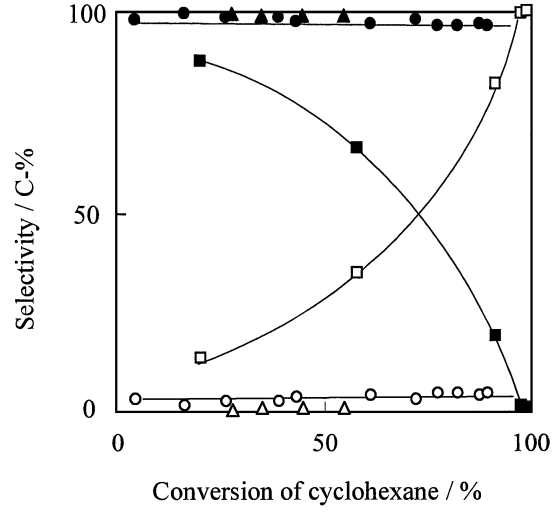

FIG. 9. Selectivity in the reaction of cyclohexane on Ni/SiO_2 (■, C_6H_6; □, CH_4), Ni_3Sn/SiO_2 (●, ○) and Ni_3Sn_2/SiO_2 (▲, △) catalysts at 773 K. $P(H_2) = 16.0$ kPa; P(cyclohexane) = 2.7 kPa.

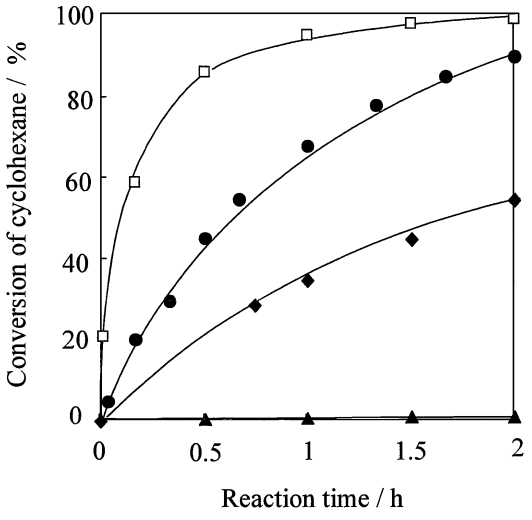

FIG. 10. Conversion of cyclohexane on Ni/SiO_2 (□), Ni_3Sn/SiO_2 (●), Ni_3Sn_2/SiO_2 (◆), and Ni_3Sn_4/SiO_2 (▲) for the reaction of cyclohexane at 773 K. $P(H_2) = 16.0$ kPa; P(cyclohexane) = 2.7 kPa.

converted cyclohexane to benzene with a small amount of cyclohexene.

Figure 10 shows the catalytic activities of supported Ni, Ni_3Sn, Ni_3Sn_2, and Ni_3Sn_4 for the reaction of cyclohexane. The order of conversion rate for cyclohexane was as follows:

$$Ni/SiO_2\ (9) > Ni_3Sn/SiO_2\ (2.5) > Ni_3Sn_2/SiO_2\ (1) > Ni_3Sn_4/SiO_2\ (0.02).$$

The relative initial conversion rates are indicated in parentheses. The activity of Ni–Sn IMC/SiO_2 was lower than that of Ni/SiO_2. The activity of Ni_3Sn_2/SiO_2 was about 2.5 times lower than that of Ni_3Sn/SiO_2 and the activity of Ni_3Sn_4/SiO_2 was about 50 times lower than that of Ni_3Sn_2/SiO_2. In the case of cyclohexane dehydrogenation over Sn deposited on Pt(111), a similar trend in activity was reported (22); that is, the ordered Sn/Pt(111) surface alloy does not have higher specific activity than Pt(111).

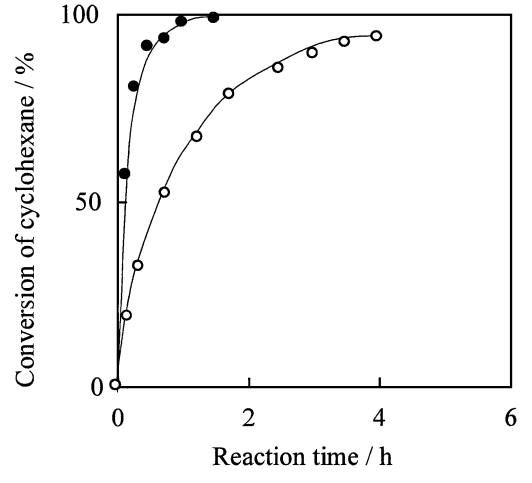

FIG. 11. Conversion of cyclohexane on Ni_3Sn/SiO_2 (●, 0.050 g) and unsupported Ni_3Sn (○, 0.50 g) at 823 K. $P(H_2) = 16.0$ kPa; P(cyclohexane) = 2.7 kPa.

Figure 11 shows dehydrogenation of cyclohexane over Ni_3Sn/SiO_2 and unsupported Ni_3Sn at 823 K. When the specific activity per weight of Ni_3Sn was obtained from the initial conversion rate, Ni_3Sn/SiO_2 was about 1000 times more active than the unsupported Ni_3Sn catalyst. When the specific surface area per weight of Ni_3Sn was obtained from the average particle sizes, Ni_3Sn particles on silica had about a 1500 times larger area than unsupported Ni_3Sn. Although the particle sizes had a wide distribution, the activity per surface area of Ni_3Sn was regarded as nearly the same as that for the supported and unsupported catalysts. In conclusion, the Ni–Sn IMC/SiO_2 catalysts prepared by CVD have high activity due to their high dispersion without losing the intrinsic selectivity of IMC catalysts.

4. CONCLUSION

Silica-supported Ni–Sn IMC catalysts with bulk Ni/Sn atomic ratios of 3/1, 3/2, and 3/4 are selectively prepared by CVD of $Sn(CH_3)_4$ onto Ni/SiO_2 at optimum temperature. These materials are composed of single phases of Ni_3Sn, Ni_3Sn_2, and Ni_3Sn_4, respectively. Ni–Sn IMC/SiO_2 catalysts have almost the same catalytic selectivity as unsupported Ni–Sn IMC in acetylene hydrogenation into ethylene and cyclohexane dehydrogenation into benzene. The Ni–Sn IMC/SiO_2 catalysts with fine IMC particles have much higher activity than the corresponding unsupported catalysts due to the much higher dispersion of IMC particles.

REFERENCES

1. Sinfelt, J. H., "Bimetallic Catalysts: Discoveries, Concepts and Applications." Wiley, New York, 1983.
2. Ponec, V., and Bond, G. C., *Stud. Surf. Sci. Catal.* **95**, 212 (1995).
3. Kappenstein, C., Guerin, M., Lazar, K., Matusek, K., and Paal, Z., *Faraday Trans.* **94**, 2463 (1998).
4. Strinivas, S. T., and Rao, P. K., *J. Catal.* **179**, 1 (1998).
5. Llorca, J., de la Piscina, P. R., Fierro, J.-L. G., Sales, J., and Homs, N., *J. Catal.* **156**, 139 (1995).
6. Huang, Z., Fryer, J. R., Park, C., Stirling, D., and Webb, G., *J. Catal.* **159**, 340 (1996).
7. Dautzenberg, F. M., Helle, J. N., Biloen, P., and Sachtler, M. H., *J. Catal.* **63**, 119 (1980).
8. Bacaud, R., Bussiere, P., and Figueras, F., *J. Catal.* **69**, 399 (1981).
9. Masai, M., Mori, K., Muramoto, H., Fujiwara, T., and Ohnaka, S., *J. Catal.* **38**, 128 (1975).
10. Wallace, W. E., *Chemtech* **12**, 752 (1982).
11. Takeshi, T., Wallace, W. E., and Craig, R. S., *J. Catal.* **44**, 236 (1976).
12. Soga, K., Imamura, H., and Ikeda, S., *J. Phys. Chem.* **81**, 1762 (1977).
13. Chojnacki, T. P., and Schmidt, L. D., *J. Catal.* **129**, 473 (1991).
14. Komatsu, T., Fukui, M., and Yashima, T., in "Proceedings, 11th International Congress on Catalysis, Baltimore, 1996" (J. W. Hightower,

W. N. Delgass, E. Iglesia, and A. T. Bell, Eds.), Stud. Surf. Sci. Catal., Vol. 101, p. 1095. in Elsevier, Amsterdam, 1991.
15. Komatsu, T., Hyodo, S., and Yashima, T., *J. Phys. Chem. B.* **101**, 5565 (1997).
16. Onda, A., Komatsu, T., and Yashima, T., *Phys. Chem. Chem. Phys.* **2**, 2999 (2000).
17. Holmblad, P. M., Larsen, J. H., Chorkedorff, I., Nielsen, R. P., Besenbacher, F., Stensgaard, I., Laegsgaad, E., Kratzer, P., Hammer, B., and Norkov, J. K., *Catal. Lett.* **40**, 131 (1996).
18. Xu, C., and Koel, B. E., *Surf. Sci.* **327**, 38 (1995).
19. Overbury, S. H., and Ku, Y., *Phys. Rev. B* **46** (12), 7868 (1992).
20. Paffett, M. T., Gebhard, S. C., Windham, R. G., and Koel, B. E., *Surf. Sci.* **223**, 449 (1989).
21. Sazanyi, J., and Paffett, M. T., *J. Am. Chem. Soc.* **117**, 1034 (1995).
22. Park, Y. K., Ribeiro, F. H., and Somorjai, G. A., *J. Catal.* **178**, 66 (1998).
23. Sazanyi, J., Anderson, S., and Paffett, M. T., *J. Catal.* **149**, 435 (1994).
24. Candy, J. P., Mansour, A. E., Ferretti, O. A., Mablion, G., Bournonville J. P., Basset, J. M., and Martino, G., *J. Catal.* **112**, 201 (1988).
25. Lesage, P., Clause, O., Moral, P., Didillon, B., Candy, J. P., and Basset, J. M., *J. Catal.* **155**, 238 (1995).
26. Tomishige, K., Asakura, K., and Iwasawa, Y., *J. Catal.* **149**, 70 (1994).
27. Santri, G. F., Casella, M. L., Siri, G. J., Aduriz, H. R., and Ferretti, O. A., *Appl. Catal. A* **197**, 141 (2000).
28. Massalski, T. B., Okamoto, H., Subramanian, P. R., and Kacprzak, L., "Binary Alloy Phase Diagrams," 2nd ed. ASM International and National Institute of Standard and Technology, Materials Park, OH, 1990.
29. Onda, A., Komatsu, T., and Yashima, T., *Chem. Commun.* 1507 (1998).
30. Nedez, C., Theolier, A., Lefebvre, F., Choplin, A., Basset, J. M., and Joly, J. F., *J. Am. Chem. Soc.* **115**, 722 (1993).
31. Inoue, T., Tomishige, K., and Iwasawa, Y., *Faraday Trans.* **92**, 461 (1996).
32. Moulder, G. E., Stickle, W. F., Sobol, P. E., and Bomben, K. D., "Handbook of X-ray Photoelectron Spectroscopy," 2nd ed. Perkin-Elmer, Physical Electronics Division, Wellesley, MA, 1992.
33. Bond, G. C., "Catalysis by Metals," Academic Press, London, 1962.